Ultramicroscopy 138 (2014) 22–27

Contents lists available at ScienceDirect

Ultramicroscopy

journal homepage: www.elsevier.com/locate/ultramic

Generation of a spin-polarized electron beam by multipole magnetic fields

Ebrahim Karimi [a,*], Vincenzo Grillo [b], Robert W. Boyd [a,c], Enrico Santamato [d,e]

[a] Department of Physics, University of Ottawa, 150 Louis Pasteur, Ottawa, Ontario, Canada K1N 6N5
[b] CNR-Istituto Nanoscienze, Centro S3, Via G Campi 213/a, I-41125 Modena, Italy
[c] Institute of Optics, University of Rochester, Rochester, NY 14627, USA
[d] Dipartimento di Scienze Fisiche, Università di Napoli "Federico II", Compl. Univ. di Monte S. Angelo, 80126 Napoli, Italy
[e] Consorzio Nazionale Interuniversitario per le Scienze Fisiche della Materia, Napoli, Italy

ARTICLE INFO

Article history:
Received 1 July 2013
Received in revised form
31 October 2013
Accepted 18 December 2013
Available online 31 December 2013

Keywords:
Electron vortex beam
Polarized electron beam
Spin-to-orbit conversion

ABSTRACT

The propagation of an electron beam in the presence of transverse magnetic fields possessing integer topological charges is presented. The spin–magnetic interaction introduces a nonuniform spin precession of the electrons that gains a space-variant geometrical phase in the transverse plane proportional to the field's topological charge, whose handedness depends on the input electron's spin state. A combination of our proposed device with an electron orbital angular momentum sorter can be utilized as a spin-filter of electron beams in a mid-energy range. We examine these two different configurations of a partial spin-filter generator numerically. The results of this analysis could prove useful in the design of an improved electron microscope.

1. Introduction

A few years ago, the existence of electron beams carrying orbital angular momentum (OAM) was predicted theoretically [1]. A couple of years later, two different techniques, based on the holography and random phase changes in a graphite sheet, were used to generate electron beams carrying OAM, i.e., electron vortex beams, experimentally [2–4]. Such an intriguing topic is of particular interest to materials scientists, since it can be used to probe the magnetic and spin-dependent properties of materials with atomic resolution [5,6]. The OAM as a "*rotational-like*" degree of freedom of an electron beam induces a *magnetic moment*, in addition to the spin magnetic moment, of up to few hundred Bohr magnetons per electron, which gives a possibility to interact with an external magnetic field [3,5]. The interaction of OAM magnetic moments with a uniform longitudinal magnetic field or a flux has been recently examined theoretically and experimentally [7–9]. This interaction enhances or diminishes the kinetic OAM of the beam, and can be used to measure or sort the OAM of electron beams spatially. However, besides its interesting and fascinated applications, this novel degree of freedom of free electrons can be utilized to investigate some fundamental quantum concepts such as the *Bohr–Pauli impossibility of generating a spin-polarized free electron beam* [10,11].

The spin–orbit coupling in a non-uniform balanced electric-magnetic field, named a "*q*-filter", was proposed by some of the authors as a novel tool to generate an electron vortex beam from a pure spin-polarized electron beam. In that configuration, the spin of an electron follows the *Larmor precession* up and acquires a geometrical phase, which depends on both the spin–magnetic field direction and the time of interaction. A non-uniform magnetic field introduces a non-uniform phase profile whose topological structure is that of the magnetic field. Several different topological charge configurations, proposed in the previous paper, have been achieved in practice [11]. A locally orthogonal electric field was proposed to compensate for the "net" magnetic force. Furthermore, the reverse process was suggested to filter the spin component of an electron beam spatially, where two different longitudinal electron's spin components suffer opposite precession directions, thus possess opposite OAM values.

In this work, we suggest a scheme based on *non-uniform magnetic fields*, rather than a balanced space-variant *Wien q*-filter, to manipulate electron OAM. Analogous to the *q*-filter, the proposed scheme imprints a topological charge – identical to the topological charge of magnetic field – onto the incoming electron beam with a handedness depending on the longitudinal component of electron spin; positive for spin up $\Uparrow\rangle$ and negative for spin down $\Downarrow\rangle$ with the advantage that no compensating electric field is needed. Unlike in the *q*-filter, however, the beam structure is now

* Corresponding author.
E-mail address: ekarimi@uottawa.ca (E. Karimi).

0304-3991/$ - see front matter © 2013 Elsevier B.V. All rights reserved.
http://dx.doi.org/10.1016/j.ultramic.2013.12.002

strongly affected by the magnetic field. A TEM_{00} Gaussian beam splits out into *multi Gaussian-like* beams after passing through the nonuniform magnetic field of the device, each beam oscillates in the opposite direction of the gradient of A_z, i.e., along $-\nabla A_z$. In particular, the incident Gaussian electron beam splits into two and three semi-Gaussian beams in quadrupole and hexapole magnetic fields, respectively. It is worth noting, however, that a multi-Gaussian-like beam does recover its original Gaussian shape at certain free-space propagation distance, provided its phase distribution does not acquire sudden changes in the transverse plane. In this work, we introduce and numerically simulate two realistic configurations of a spin-filter for electron beams, based on the new proposed device. Our numerical simulations confirm that a portion of the electrons, typically small, remains polarized after passing through the device and can be easily separated form the rest of the beam by suitable apertures.

2. Propagation of electron beams in an orthogonal uniform magnetic field

Let us assume that the electron beam moves along the z-direction perpendicular to a uniform magnetic field $\boldsymbol{B}=B_0(\cos\theta, \sin\theta, 0)$, which lies in the (x,y) transverse plane at angle θ with respect to the x-axis. As associated vector potential we may take $\boldsymbol{A}=B_0(0,0,y\cos\theta - x\sin\theta)$. We assume a nonrelativistic electron beam, so that we can use Pauli's equation

$$i\hbar\,\partial_t\tilde{\psi}=\left\{\frac{1}{2m}(-i\hbar\nabla-e\boldsymbol{A})^2-\boldsymbol{B}\cdot\hat{\boldsymbol{\mu}}\right\}\tilde{\psi}, \tag{1}$$

where $\tilde{\psi}$ is a two-component spinor and $\hat{\boldsymbol{\mu}}=\frac{1}{2}g\mu_B\hat{\boldsymbol{\sigma}}$ is the electron magnetic moment, $\mu_B=\hbar e/2m$ is Bohr's magneton, g is the electron g-factor, and $\hat{\boldsymbol{\sigma}}=(\hat{\sigma}_x,\hat{\sigma}_y,\hat{\sigma}_z)$ is Pauli's vector, respectively. We assume a paraxial beam with average linear momentum p_c and average energy $E_c=p_c^2/2m$, so that $\tilde{\psi}(x,y,z,t)=\exp[i\hbar^{-1}(p_cz-E_ct)]\tilde{u}(x,y,z)$, with $\tilde{u}(x,y,z)$ a slow-envelope spinor field [1]. Inserting this *ansatz* into Eq. (1) and neglecting the second derivatives of $\tilde{u}$ with respect to z, we obtain the paraxial Pauli equation

$$\left\{2ik_c\partial_z+\nabla_\perp^2+2k_c\frac{e}{\hbar}A-\frac{e^2}{\hbar^2}A^2+\frac{2m}{\hbar^2}\boldsymbol{B}\cdot\hat{\boldsymbol{\mu}}\right\}\tilde{u}(x,y,z)=0, \tag{2}$$

where $\perp$ stands for the transverse coordinate, and $k_c=p_c/\hbar$ is the central de Broglie wave-vector.

Eq. (2) is solved with initial Cauchy data at $z=0$, $\tilde{u}(r,\phi,0)=\tilde{a}\exp(-r^2/w_0^2)$ corresponding to a Gaussian beam of width w_0 in the cylindrical coordinates of (r,ϕ,z). The constant spinor $\tilde{a}=(a_1,a_2)$ describes the polarization state $|\psi\rangle=a_1|\Uparrow\rangle+a_2|\Downarrow\rangle$ of the input beam in the $|\Uparrow\rangle$, $|\Downarrow\rangle$ basis where the spin is aligned parallel or antiparallel to the beam propagation direction, respectively. We assume the normalization $|a_1|^2+|a_2|^2=1$. A straightforward calculation shows that the required solution of the paraxial Pauli equation is given by

$$\tilde{u}(r,\phi,z)=G(r,\phi,z)\hat{M}(z)\tilde{a}, \tag{3}$$

where $\hat{M}(z)$ is a matrix given by

$$\hat{M}(z)=\begin{pmatrix}\cos\frac{2\pi z}{\Lambda_1} & ie^{-i\theta}\sin\frac{2\pi z}{\Lambda_1}\\ ie^{i\theta}\sin\frac{2\pi z}{\Lambda_1} & \cos\frac{2\pi z}{\Lambda_1}\end{pmatrix}, \tag{4}$$

with $\Lambda_1=4\pi\hbar^2k_c/mg\mu_BB_0$. The matrix $\hat{M}(z)$ accounts for the action of the magnetic field on the particle spin. The action on the electron motion is described in Eq. (3) by the Gaussian-coherent factor $G(r,\phi,z)$ given by

$$G(r,\phi,z)=\sqrt{\frac{-k_cz_R}{\pi q_\parallel(z)q_\perp(z)}}\,e^{ik_c(f_g(r,\phi)/2q_\parallel(z)+f_c(r,\phi,z)/2q_\perp(z)+z/2)} \tag{5}$$

with

$$\begin{aligned}f_g(r,\phi)&=r^2\cos^2(\theta-\phi),\\ f_c(r,\phi,z)&=i\left(\frac{\pi}{\Lambda}\right)\left(\frac{\Lambda}{\pi}+r\sin(\theta-\phi)\right)\\ &\times\left(2i\left(\frac{\Lambda}{\pi}\right)^2+\left(\frac{\pi}{\Lambda}\right)z_R\left(q_\perp(z)+iz_R\cos\left(\frac{\pi z}{\Lambda}\right)\right)\right.\\ &\times\left.\left(\frac{\Lambda}{\pi}+r\sin(\theta-\phi)\right)\right)+\cos\left(\frac{\pi z}{\Lambda}\right)\\ &\times\left(2\left(\frac{\Lambda}{\pi}\right)^2+r\sin(\theta-\phi)\left(2\left(\frac{\Lambda}{\pi}\right)+r\sin(\theta-\phi)\right)\right).\end{aligned} \tag{6}$$

The complex curvature radii of the Gaussian-coherent factor $G(r,\phi,z)$ are given by

$$q_\parallel(z)=z-iz_R \tag{7}$$

$$q_\perp(z)=\left(\frac{\Lambda}{\pi}\right)\sin\left(\frac{\pi z}{\Lambda}\right)-iz_R\cos\left(\frac{\pi z}{\Lambda}\right), \tag{8}$$

where $z_R=\frac{1}{2}k_cw_0^2$, $\Lambda=\pi\hbar k_c/eB_0$. From Eq. (4) we see that the beam spin state oscillates during propagation with spatial period Λ_1.

Moreover, unlike the case with the Wien-filter, in which the mean direction of the beam is not affected, now the beam oscillates perpendicularly to the magnetic field $\boldsymbol{B}$ towards $-\nabla A_z$ with spatial period $2\Lambda=(g/4)\Lambda_1\simeq\Lambda_1/2\propto B_0^{-1}$. Fig. 1(a) shows the beam intensity profiles at two different z-planes; at the entrance plane $z=0$ (central spot) and at $z=\alpha\Lambda$ with $\alpha=0.44\%$ (upper spot). The electron trajectory in the yz-plane, orthogonal to the magnetic field, is shown in Fig. 1(b): the electron beam follows a sinusoidal oscillation with spatial period 2Λ and amplitude $2\Lambda/\pi$.

3. Propagation of electron beams in an orthogonal nonuniform magnetic field possessing a specific topological charge

Eq. (3) represents an exact solution of the beam paraxial equation, with explicit boundary conditions, for a uniform constant magnetic field at angle θ with respect to the x-axis. If the angle $\theta=\theta(x,y)$ changes slowly in the transverse plane, we may assume that the solution (3) is still approximately valid. This Geometric Optics Approximation (GOA) is quite accurate in the present case, since the electron beam wavelength in a typical Transmission Electron Microscope (TEM) is in the range of tens of picometers, while θ changes over length of several microns. Within this slowly varying approximation, the effect of a nonuniform magnetic field is obtained simply by replacing θ with $\theta(x,y)$ in Eqs. (4)–(6). We assume a singular space distribution of the magnetic field where $\theta(x,y)=\theta(r,\phi)$ is given by

$$\theta(\phi)=q\phi+\beta, \tag{9}$$

where $\phi=\arctan(y/x)$ is the azimuthal angle in the beam transverse plane and β is a constant angle, which defines the inclination on the x-axis. Finally q is an integer which fixes the topological charge of the singular magnetic field distribution. Such magnetic structures can be generated in practice by multipolar lenses (for negative charges q) or by a set of appropriate longitudinal currents at origin (for positive

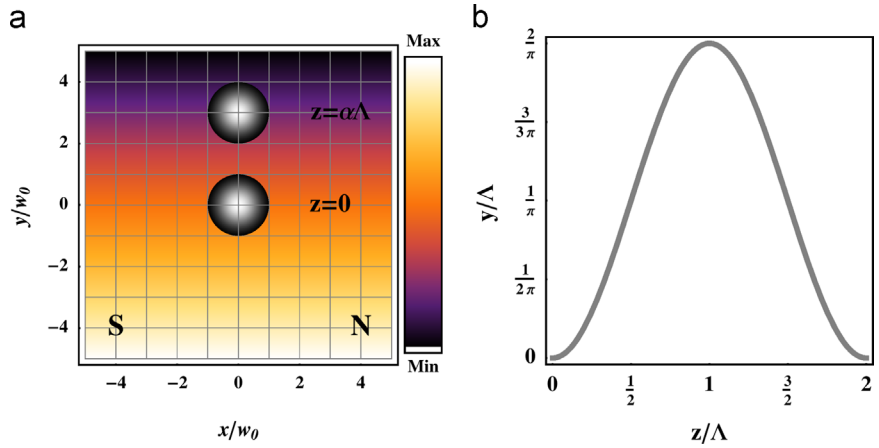

Fig. 1. (a) Cross section of an electron Gaussian beam propagating in a uniform magnetic field along the x-axis. During propagation the beam starts to move up in the positive y-direction, orthogonal to the magnetic field. The figure shows the beam position at $z=\alpha\Lambda$ with $\alpha=4.4\times10^{-3}$. The sidebar shows the strength of the vector potential in false-color. (b) y-displacement of the beam center as a function of the z coordinate. The oscillation is sinusoidal and recovers its transverse position and shape at planes $z=n\Lambda$ (n integer). The simulation was performed for an electron beam having energy $E_c=100$ keV and waist $w_0=10$ μm, in a magnetic field of strength $B_0=3.5$ mT.

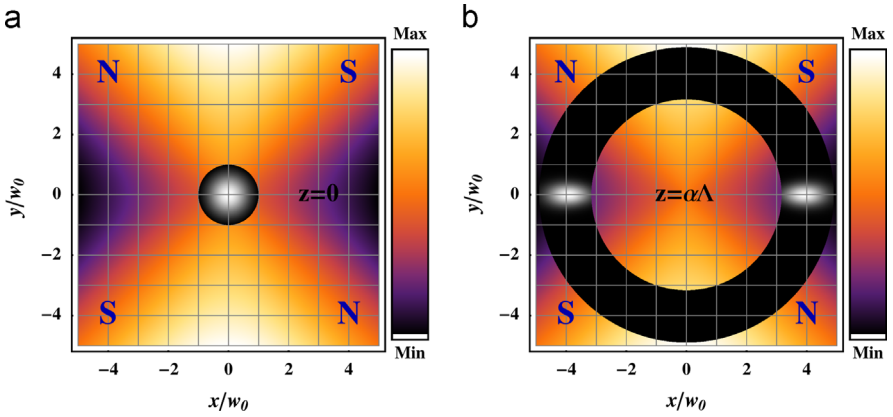

Fig. 2. Propagation of an electron Gaussian beam through a quadrupole ($q=-1$ and $\beta=-\pi/2$) magnetic field; (a) at the quadrupole pupil, (b) after a propagation distance given by $z=\alpha\Lambda$. As shown in (b), the beam splits out into two different astigmatic quasi-Gaussian beams along $-\nabla A_z$ inside the quadrupole, along x-axis. The bar side shows the strength of the vector potential in false-color. Simulation was performed for $\alpha=4.4\times10^{-3}$.

charge q). Inserting Eq. (9) into Eqs. (4) and (6) yields

$$\hat{M}(z)=\begin{pmatrix}\cos\frac{2\pi z}{\Lambda_1} & ie^{-iq\phi}e^{-i\beta}\sin\frac{2\pi z}{\Lambda_1}\\ ie^{iq\phi}e^{i\beta}\sin\frac{2\pi z}{\Lambda_1} & \cos\frac{2\pi z}{\Lambda_1}\end{pmatrix} \tag{10}$$

and

$$\begin{aligned}f_g(r,\phi)&=r^2\cos^2((q-1)\phi+\beta),\\ f_c(r,\phi,z)&=i\left(\frac{\pi}{\Lambda}\right)\left(\frac{\Lambda}{\pi}+r\sin((q-1)\phi+\beta)\right)\\ &\times\left(2i\left(\frac{\Lambda}{\pi}\right)^2+\left(\frac{\pi}{\Lambda}\right)z_R\left(q_\perp(z)+iz_R\cos\left(\frac{\pi z}{\Lambda}\right)\right)\right.\\ &\times\left.\left(\frac{\Lambda}{\pi}+r\sin((q-1)\phi+\beta)\right)\right)+\cos\left(\frac{\pi z}{\Lambda}\right)\\ &\times\left(2\left(\frac{\Lambda}{\pi}\right)^2+r\sin((q-1)\phi+\beta)\right.\\ &\times\left.\left(2\left(\frac{\Lambda}{\pi}\right)+r\sin((q-1)\phi+\beta)\right)\right).\end{aligned} \tag{11}$$

Eq. (10) shows that in passing through a multipole magnetic field of length L, a fraction $|\eta|^2=|\sin(2\pi L/\Lambda_1)|^2$ of the electrons in the beam flip their spin and acquire a phase factor $\exp(\pm iq\phi)$ according to whether the initial spin was up $|\uparrow\rangle$ or down $|\downarrow\rangle$. The rest of the electrons, i.e., $1-|\eta|^2$, pass through without changing their initial spin state. When $L=\Lambda_1/2$ (mod 2π), all electrons emerge with their spins reversed and acquire the abovementioned phase factor, which means that an amount of $\pm\hbar q$ is added to their initial OAM value. In this case the Spin-To-OAM Conversion (STOC) process is complete and we say that the device is "*tuned*" [11]. Tuning can be achieved by altering the strength of the magnetic field or changing the device length. The STOC process is governed by the $\exp(\pm iq\phi)$ factors in Eq. (10), which is of geometrical origin [12]. As a consequence, the STOC process occurs even if the field amplitude B_0 is (slowly) dependent on the radial coordinate r in the beam transverse plane. The capability of changing the electron OAM and of creating a correlation between OAM and spin are the main features of the non-uniform magnetic multipoles. Eq. (11) shows that the device significantly alters the transverse profile of the beam which acquires multi quasi-Gaussian shapes as shown in Figs. 2(b) and 3(b) for quadrupole and hexapole magnetic field, respectively. The initial Gaussian beam breaks up upon propagation through the magnetic field into two and three astigmatic quasi-Gaussian beams for quadrupole and hexapole, respectively. The cleft number depends on the number of local vector potential minima. Both the STOC and non-STOC parts of the beam possess the same intensity profile; but the STOC part only acquires a helical phase structure according

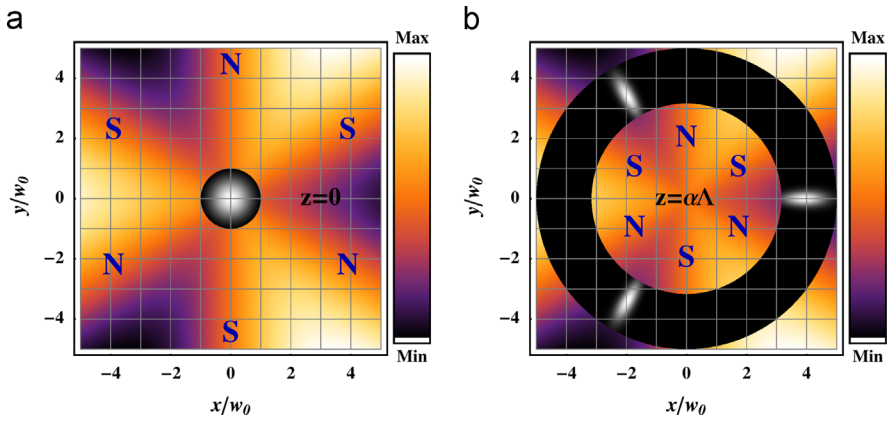

Fig. 3. Propagation of an electron gaussian beam through a hexapoles ($q=-2$ and $\beta=-\pi/2$) magnetic field; (a) at the pupil of hexapoles, (b) after a propagation distance of $z=\alpha\Lambda$. As shown, during propagation the beam splits out into three different astigmatic quasi-Gaussian beams along $-\nabla A_z$. The bar side shows the strength of the vector potential in false-color. The simulation was been performed for $\alpha=4.4\times10^{-3}$.

to the magnetic field topological charge. For a small beam distortion, it can be shown that in the far-field the multi-Gaussian-like beam with the helical structure assumes a doughnut shape, while the vortex free non-STOC beam assumes a Gaussian shape.

4. Fringe fields and their effect on spin-filtering

In practice, it is impossible to generate a completely transverse magnetic field. Further non-transverse components, known as *fringe fields*, cannot be avoided. In this section, we examine the effect of the fringe fields on the spatial distribution of an electron beam when our proposed device is not tuned. A non-tuned device, based on its length and magnetic field strength, converts only a portion of the incoming beam – the remaining part of the beam left unchanged. When the non-tuned device is applied to an unpolarized electron beam, the beam exits in a mixture state of spin *up* and *down* with opposite OAM values, given by

$$|\psi\rangle_{\mathrm{STOC}}=\eta\begin{cases}|\uparrow,-\ell\rangle & \text{for spin } |\downarrow\rangle \text{ input},\\ |\downarrow,+\ell\rangle & \text{for spin } |\uparrow\rangle \text{ input},\end{cases} \tag{12}$$

where $|\ell\rangle$ stands for the OAM state given by topological charge of device, i.e., $\ell=q$, and $|\eta|^2=|\sin(2\pi L/\Lambda_1)|^2$ is the device STOC's efficiency. The main fringe fields appear at the entrance and the exit face of the device as nonuniform longitudinal magnetic fields. The interaction of longitudinal magnetic field with both spin and orbital angular momentum of electron beams has been recently theoretically investigated [8]. The longitudinal magnetic field introduces a phase rotation $\Phi(\ell,s)\propto B_z(\ell+gs)z$ on the beam, where $s=\pm1$ is the spin eigenvalues in units of $\hbar/2$ corresponding to spin *up* and *down*, respectively, and B_z is in general a function of transverse radial coordinate r [8]. This phase rotation comes out from the Zeeman interaction. The longitudinal fringe field introduces a different phase change in each term of Eq. (12) which is therefore changed into

$$|\psi\rangle_{\mathrm{STOC}}=\eta\begin{cases}e^{i\Phi(-\ell,1)}|\uparrow,-\ell\rangle & \text{for spin } |\downarrow\rangle \text{ input}\\ e^{i\Phi(\ell,-1)}|\downarrow,+\ell\rangle & \text{for spin } |\uparrow\rangle \text{ input}.\end{cases} \tag{13}$$

Since the fringe fields are nonuniform, in general, the phases in Eq. (13) are coordinate dependent and produce dual converging and diverging astigmatic effects. However, even in the presence of fringe fields, the two spin states of the emerging beam are still labeled by the two values $\pm\ell$ of OAM so that an OAM sorter can be used to separate the electrons according to their spin value. In the next section, we determine numerically the efficiency of this method of obtaining polarized electron beams by using a pitchfork hologram with topological charge ℓ as an OAM sorter. The final state after an OAM sorter, then, is

$$|\psi\rangle_{\mathrm{final}}=\eta\begin{cases}e^{i\Phi(-\ell,1)}|\uparrow,0\rangle & \text{for spin } |\downarrow\rangle \text{ input}\\ e^{i\Phi(\ell,-1)}|\downarrow,+2\ell\rangle & \text{for spin } |\uparrow\rangle \text{ down}.\end{cases} \tag{14}$$

The first term tends to recover the Gaussian shape, while the second term will have a doughnut shape in the far-field. Both of the non-STOC terms posses OAM$=\ell$ since the hologram, i.e., OAM sorter, is spin independent. A spatial selector, e.g. a pinhole, can be used to select the central part, which has a uniform coherent spin *up* state. The efficiency and purity of the spin filter depends on the pinhole radius, which for an optical field has been discussed in [13]. Thus, a combination of this device with an OAM sorter yields an electron spin-filter that is practical, since the multipolar magnetic magnets are available commercially as aberration correctors for TEM as well as OAM sorters.

5. Numerical simulation and technical discussions

The GOA analytical solution presented in Section 2 may be used to obtain preliminary information on the STOC efficiency and beam intensity profile in the device. However, more details on the interaction of a space-variant magnetic field with an electron beam can be examined by implementing both a ray tracing technique and the spin–orbit interaction simultaneously. In order to overcome this issue, we developed a research software based on the *multi-slice method* used in electron microscopy, where Eq. (2) has been considered as a free particle motion under the force of a "*local potential*" of A, A^2 and Pauli terms. Therefore, one can evolve both temporal and z-dependence of the wave-function based on a well-known *Dyson*-like decomposition, since both operators of the scalar wave equation and local potential do not commute [14,15]. The potential was divided and projected onto multi-slices where the beam wave-function was constructed by free-space propagation between each slice. After each iteration the wave-function turns into

$$u(\mathbf{r}_\perp,z_{j+1})=\mathcal{K}\otimes\left(e^{((i/\hbar v)\int_{z_j}^{z_{j+1}}V(\mathbf{r}_\perp,\zeta)d\zeta)}\cdot u(\mathbf{r}_\perp,z_j)\right), \tag{15}$$

where v is the electrons velocity, $\otimes$ is the convolution with the wave-function inside parentheses, z_j and $V(\mathbf{r}_\perp,\zeta)$ stand for position of jth slice and the local potential (third, fourth and fifth term of Eq. (2)), respectively (see Ref. [16] for more details). $\mathcal{K}$ is the Fresnel propagator between each two adjacent slices spaced by

Δz, which is given by

$$\mathcal{K} = \frac{-ik_c}{2\pi\Delta z} e^{(ik_c/2\Delta z)(x^2+y^2)}. \quad (16)$$

Apart from the simple concept, one may extend such a powerful algorithm to the relativistic case as well [17]. However, since electron microscopes work at mid-range energy, our simulation was carried out in the non-relativistic regime. We considered two possible configurations to generate a spin-polarized electron beam in an electron microscope.

(i) A first scheme can in principle be adopted in various microscopes using a condenser stigmator. In this first scheme, a Gaussian beam is directed to a quadrupolar magnetic field, and then to a pitch-fork hologram as shown in Fig. 4. A lens condenser can be used to form the far-field image of the hologram. However, the intensity required for the magnetic field could make the operation difficult. It also turns out that it is difficult to polarize electrons before the specimen, except in microscopes with two or even three condenser aperture planes. On the other hand, different spin states can be selected by looking at counterpart diffraction orders. Thus, first and minus first orders after being spatially selected possess different spins, i.e., *up* and *down*, suitable for examining the spin dependence of materials. Moreover, both beams can be used to perform interference experiments with two spin states to reveal the degree of polarization.

The simulated electron beam shapes after passing through the quadrupole and the pitch-fork hologram for spin *up* and *down* input are shown in Fig. 5.

The first and second rows in Fig. 5 show the far-field intensity pattern for input electrons with spin *up* and *down* states, respectively. The subrows correspond to expected spin states for the first order of diffraction (left spots). The non-STOC part of both spin *up* and *down*, i.e., first and last rows of Fig. 5, forms a *Hermite-Gaussian* shape of first order, which is affected by the quadrupole's astigmatism and splits into two parts. Conversely the STOC parts are shaped differently depending on the initial spin state; one as the *Hermite-Gaussian* of second order while the other one forms a Gaussian beam bearing some astigmatic distortion. It can be seen that an aperture with appropriate size can be used to select the central spot only, which possesses opposite polarizations.

(ii) In the second method, a simplified scheme of a spherical aberration corrector is considered, see Fig. 6. Indeed, normal Cs-

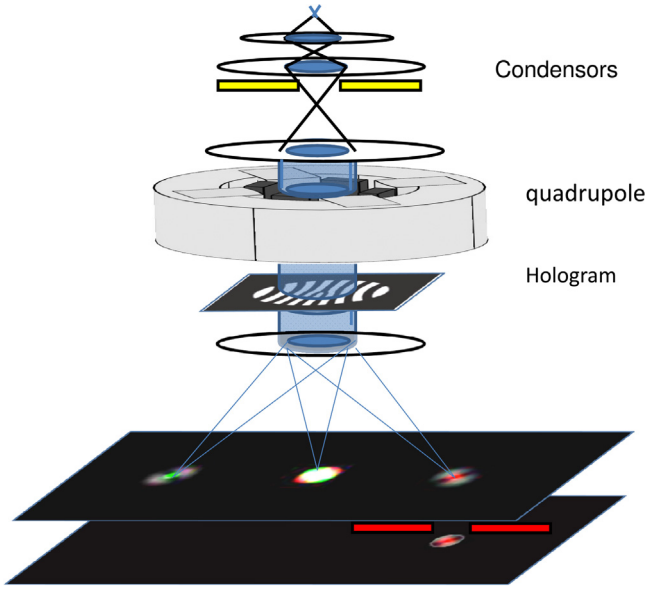

Fig. 4. First proposed scheme to generate a spin-polarized electron beam based on space-variant magnetic fields.

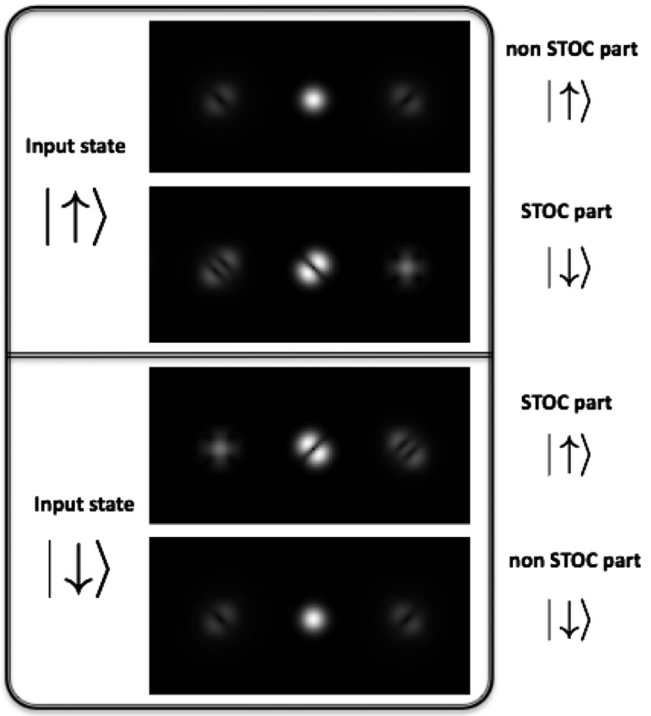

Fig. 5. Simulated diffraction pattern of the beam generated by a quadrupole after passing through a pitch-fork hologram (right spot assumed to be the first order of diffraction). In a fraction of the beam the nonuniform magnetic field of the quadrupole couples electron spin to OAM. Up and down subfigures inside each row show the non-converted and converted parts of an input 50–50 mixture of spin *up* and *down*, respectively. The electrons' spin state in the first order of diffraction has been indicated at the right side of images.

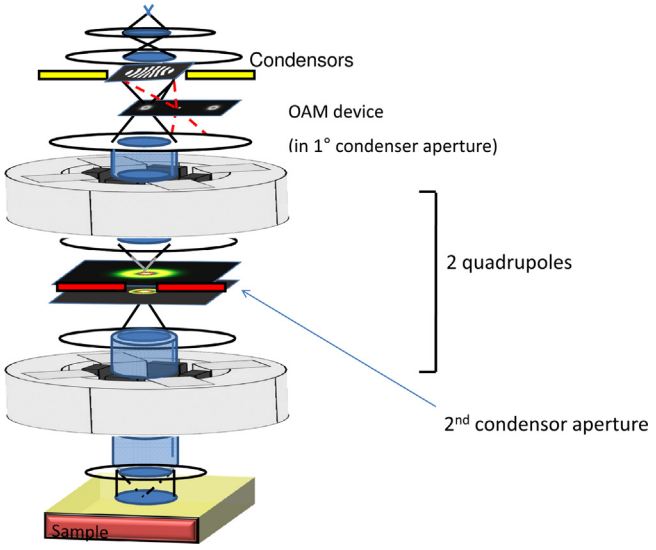

Fig. 6. Second proposed scheme to generate a spin-polarized electron beam based on coupling with two magnetic quadrupoles (spherical aberration corrector). The second quadrupole corrects the aberration induced by the first one. Nevertheless, the spin-to-orbit coupling efficiency after the second quadrupole can be completely neglected.

correctors contain, as main elements, a set of opposite hexapoles [18]. However, in order to simplify the numerical calculations, we substituted them with quadrupoles. In this sense a set of coupled quadrupoles would probably do the same job but given large diffusion of Cs-corrector it appears interesting to refer also to this device. Therefore, we assume that two quadrupoles with opposite

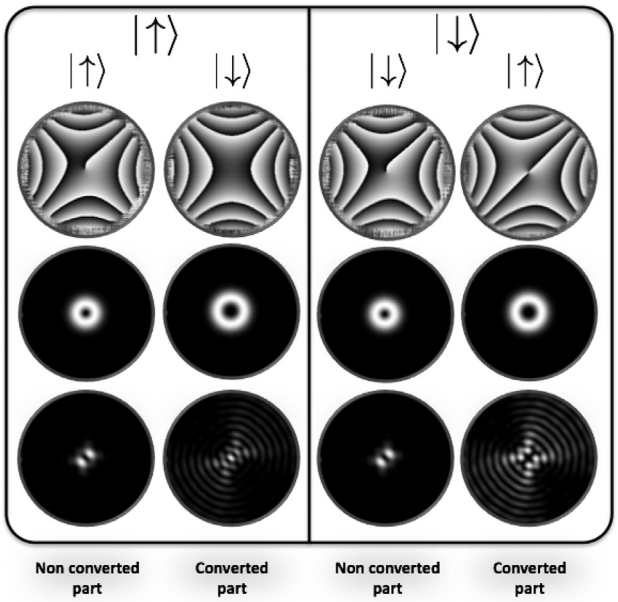

Fig. 7. As the beam with OAM = +1 propagates inside the aberration corrector system (quadrupole–condenser–aperture and a rotated quadrupole), it sees an astigmatism effect introduced by the quadrupoles and, based on the time interaction, a portion of electrons undergo spin-to-orbit conversion (second and fourth column). The first two rows show phase and intensity distributions of the electron beam after the first quadrupole for a mixture of 50–50 spin *up* and *down*, respectively. The last row shows output intensity distributions for both the converted and non-converted parts of spin up and down after interacting with the whole system. The simulation was carried out for an input electron beam size of 1 μm, a quadrupole magnetic field of 0.1 mT at the beam waist radius, and a device thickness of 10 μm. This relatively small thickness was chosen to simplify and speed up the numerical calculation and to avoid too large phase deformations.

polarizations are coupled through two cylindrical lenses (transport lenses) having magnetic fields along the propagation direction. Different from the real device, we assume that a limiting aperture can be added inside the corrector in correspondence to the focal plane of the transport lenses. Fig. 7 shows the simulated evolution of the wave-function in the system for both spins. At the exit face of the first quadrupole the two polarizations are indistinguishable, but evolve to different intensity distributions in the focal plane where an aperture selects the central part of the beam containing mainly the $\Uparrow,0\rangle$ electron state. The second quadrupole, indeed, implies aberration correction into the selected $\Uparrow,0\rangle$ beam. It is worth noticing that spin-to-orbit coupling after the second quadrupole can be neglected, due to the strength of the magnetic field.

6. Conclusions

We presented two possible practical devices to generate a spin polarized electron beam via a spin-to-orbit conversion in the presence of a nonuniform transverse magnetic field. The main component of both devices is a multipolar magnet generating a singular transverse magnetic structure with negative integer topological charge. The device action on a pure spin-polarized electron beam is to induce spin-to-orbit conversion, whereby the beam gains a nonuniform phase structure which is defined by the magnetic field topological charge, where the sign is given by the input electron spin value. When the device is combined with an OAM sorter, spiral phase plate, hologram, or even a longitudinal magnetic field, it can be used as a spin-filter to polarize the electron beam. However, because of the strong astigmatism, the efficiency of the devices proposed here are lower than the ones discussed in Ref. [11]. Finally, it is worth mentioning that the purity of the generated polarized electrons is reasonably higher than other proposed approaches such as the spin-dependent scattering process in diamond loops, and implementing a different photocathode [19,20].

Acknowledgment

V.G. would like to thank Prof. M. Heider and Dr. H. Mueller for useful discussion. E.K. and R.W.B. acknowledge the support of the Canada Excellence Research Chairs (CERC) program. E.S. acknowledges the financial support of the Future and Emerging Technologies (FET) programme within the Seventh Framework Programme for Research of the European Commission, under FET-Open grant number 255914-PHORBITECH.

References

[1] K.Y. Bliokh, Y.P. Bliokh, S. Savel′ev, F. Nori, Semiclassical dynamics of electron wave packet states with phase vortices, Phys. Rev. Lett. 99 (2007) 190404.
[2] M. Uchida, A. Tonomura, Generation of electron beams carrying orbital angular momentum, Nature (London) 464 (2010) 737–739.
[3] B.J. McMorran, A. Agrawal, I.M. Anderson, A.A. Herzing, H.J. Lezec, J.J. McClelland, J. Unguris, Electron vortex beams with high quanta of orbital angular momentum, Science 331 (2011) 192–195.
[4] J. Verbeeck, H. Tian, P. Schattschneider, Production and application of electron vortex beams, Nature (London) 467 (2010) 301–304.
[5] J. Verbeek, P. Schattschneider, S. Lazar, M. Stoger-Pöllach, S. Löffler, A. Steiger-Thirsfeld, G. Van Tendeloo, Atomic scale electron vortices for nanoresearch, Appl. Phys. Lett. 99 (2011) 203109.
[6] P. Schattschneider, B. Schaffer, I. Ennen, J. Verbeeck, Phys. Rev. B 85 (2012) 134422.
[7] K.Y. Bliokh, P. Schattschneider, J. Verbeeck, F. Nori, Electron vortex beams in a magnetic field: a new twist on landau levels and Aharonov–Bohm states, Phys. Rev. X 2 (2012) 041011.
[8] C. Greenshields, R.L. Stamps, S. Franke-Arnold, Vacuum Faraday effect for electrons, New J. Phys. 14 (2012) 103040.
[9] G. Guzzinati, P. Schattschneider, K. Bliokh, F. Nori, J. Verbeeck, Observation of the Gouy and Larmor rotations in electron vortex beams, Phys. Rev. Lett. 110 (2013) 093601.
[10] O. Darrigol, A history of the question: can free electrons be polarized? Hist. Stud. Phys. Sci. 15 (1984) 39–79.
[11] E. Karimi, L. Marrucci, V. Grillo, E. Santamato, Spin-to-orbital angular momentum conversion and spin-polarization filtering in electron beams, Phys. Rev. Lett. 108 (2012) 044801.
[12] L. Marrucci, E. Karimi, S. Slussarenko, B. Piccirillo, E. Santamato, E. Nagali, F. Sciarrino, Spin-to-orbital conversion of the angular momentum of light and its classical and quantum applications, J. Opt. 13 (2011) 064001.
[13] E. Karimi, B. Piccirillo, E. Nagali, L. Marrucci, E. Santamato, Efficient generation and sorting of orbital angular momentum eigenmodes of light by thermally tuned q-plates, Appl. Phys. Lett. 94 (2009) 231124.
[14] J.M. Cowley, A.F. Moodie, The scattering of electrons by atoms and crystals. I. A new theoretical approach, Acta Crystallogr. 10 (1957) 609–619.
[15] G. Pozzi, A multislice approach to magnetic electron lens theory, Ultramicroscopy 30 (1989) 417–424.
[16] V. Grillo, L. Marrucci, E. Karimi, R. Zanella, E. Santamato, Quantum simulation of a spin polarization device in an electron microscope, New J. Phys. 15 (2013) 093026.
[17] A. Rother, K. Scheerschmidt, Relativistic effects in elastic scattering of electrons in TEM, Ultramicroscopy 109 (2009) 154–160.
[18] H. Müller, S. Uhlemann, P. Hartel, M. Haider, Advancing the hexapole Cs-corrector for the scanning transmission electron microscope, Microsc. Microanal. 12 (2006) 442–455.
[19] A. Aharony, Y. Tokura, G.Z. Cohen, O. Entin-Wohlman, S. Katsumoto, Filtering and analyzing mobile qubit information via Rashba–Dresselhaus–Aharonov–Bohm interferometers, Phys. Rev. B 84 (2011) 035323.
[20] M. Kuwahara, S. Kusunoki, X.G. Jin, T. Nakanishi, Y. Takeda, K. Saitoh, T. Ujihara, H. Asano, N. Tanaka, 30-kV spin-polarized transmission electron microscope with GaAs–GaAsP strained superlattice photocathode, Appl. Phys. Lett. 101 (2012) 033102.